Geochemistry and geochronology of native copper mineralization related to the Emeishan flood basalts, Yunnan Province, China

Zhu Bing-Quan [a,*], Hu Yao-Guo [a], Zhang Zheng-Wei [a,b], Cui Xue-Jun [a], Dai Tong-Mo [a], Chen Guang-Hao [a], Peng Jian-Hua [b], Sun Yong-Ge [a], Liu De-Han [a], Chang Xiang-Yang [a]

[a] Guangzhou Institute of Geochemistry, Chinese Academy of Sciences, Guangzhou, 510640, People's Republic of China
[b] Institute of Geochemistry, Chinese Academy of Sciences, Guiyang, 550002, People's Republic of China

Abstract

Native copper mineralization in northeastern Yunnan is related to the Emeishan flood basalts, which have high Cu background concentrations. The deposits are located in the Ludian, Maoling and Yiche synclines between the flood basalts and the overlying Xuanwei Formation. Evidence from REE and HSFE concentrations, oxygen isotope compositions, bitumen reflectance, and mineral paragenesis indicates that the high-grade copper orebodies were deposited from moderate to low temperature hydrothermal solutions (420 to 100 °C) in a reducing environment. $^{40}Ar/^{39}Ar$ spectra for the laumontites that coexist with native copper in the high-grade ores yield consistent plateau and isochron ages (226 to 228 Ma). These are interpreted to represent the age of the first stage of hydrothermal mineralization, which took place at temperatures of 200 to 350 °C, concordant with that of Zn–Pb–Ag–Ge mineralization also occurring in the area. The heulandites yield a stable $^{40}Ar/^{39}Ar$ plateau age of 134.0 ± 1.7 Ma, consistent with isochron ages indicated by U–Th–Pb isotopic systematics, indicating a second stage of native copper mineralization at lower temperatures (100 to 200 °C) that took place during the Early Cretaceous.
© 2006 Elsevier B.V. All rights reserved.

Keywords: Native copper; $^{40}Ar/^{39}Ar$ geochronology; Flood basalt; Emeishan; China

1. Introduction

Cu–Ni–PGE sulfide, Fe–Ti–V oxide, native Cu–Ag and Zn–Pb–Ag–Ge sulfide mineralization are commonly related to continental flood basalts (CFB). Large deposits of these metals have been found, for example, in the Midcontinent, Siberia, Emeishan and Newark CFB provinces. Copper mineralization in CFB provinces, in which native copper is the major ore mineral, such as the Keweenaw district, U.S.A., are scarce

(Lefebure and Church, 1996; Cannon et al., 1999). Although research on these deposits has continued for about eighty years, questions remain about the source of Cu and relationship of ore to CFB magmatism, hydrothermal activity, and organic matter (Hamilton, 1967; Bornhorst et al., 1988; Davis and Paces, 1990; Ho et al., 1990; Lefebure and Church, 1996; Ho and Mauk, 1996; Zhu et al., 2003; Li et al., 2004). In this study, we focus on native copper mineralization in northeastern Yunnan Province, China (Zhu et al., 2003), which is very similar to that in the Keweenaw region. Our data provide new information on the age and geologic setting of these important deposits.

* Corresponding author.
  E-mail address: bqzhu@gig.ac.cn (Z. Bing-Quan).

2. Geological setting

The area of native copper mineralization in Sichuan, Yunnan and Guizhou provinces is situated at the triple junction of the Yangtze, Cathaysia and Indochina Blocks (Fig. 1a). The area has undergone four CFB eruption cycles that are found in four Upper Permian stratigraphic units that make up the Emeishan CFB.

From the lower to upper part, these units are the $P_2\beta_1$, $P_2\beta_2$, $P_2\beta_3$ and $P_2\beta_4$ (Guizhou Bureau of Geology and Mineral Resources, 1990; Yunnan Bureau of Geology and Mineral Resources, 1990). The fourth eruption cycle ($P_2\beta_4$), which covers an area of about 150,000 km^2, has high-Ti–P (TiO$_2$ > 3%; P$_2$O$_5$ > 0.35%) features (Zhu et al., 2005a,b), and comprises a massive basalt bed in the lower part and pyroclastic bed including
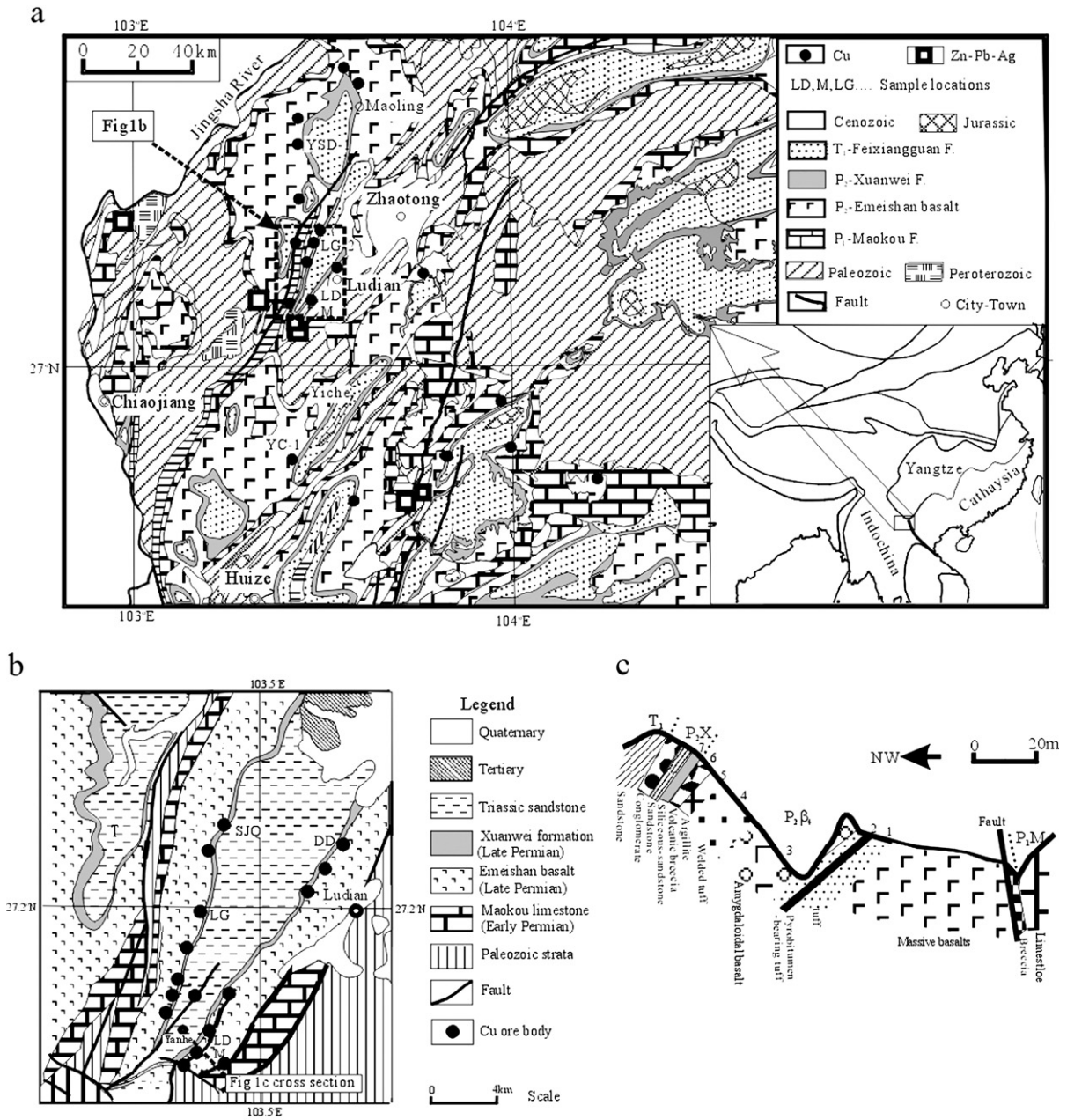

Fig. 1. a. Geological and sample location map of native copper mineralization in northeastern Yunnan Province, China. b. Geological map of the Ludian syncline. c. Cross section of Cu mineralization at the southeastern side of the Ludian syncline. Abbreviations and numbers are the names of orebodies. DD—Dadi, LD—upper part of Laoyingyan, M—middle part of Laoyingyan, LG—Longjinggou, SJQ—Sujiaqing, YSD—Yongshunde, YC—Yiche.

volcanic breccia, tuff and vesicular lava at upper levels. The Emeishan CFB is overlain by the Upper Permian Xuanwei Formation, a terrestrial coal-bearing clastic sequence (including silicalite, conglomerate, sandstone and coal beds), and is underlain by the Early Permian Maokou Formation, which consists of carbonates (Guizhou Bureau of Geology and Mineral Resources, 1990; Yunnan Bureau of Geology and Mineral Resources, 1990). The overlying Lower Triassic Feixianguan Formation consists of terrestrial sandstones and shales that were deposited in small basins (Fig. 1a). U–Pb and $^{39}Ar/^{39}Ar$ ages indicate that the Emeishan CFB has an eruption age range of 251 to 259 Ma (Zhou et al., 2002; Lo et al., 2002; Boven et al., 2002).

The major tectonic systems in the area comprise the Ludian, Maoling and Yiche synclines that strike NNE, and a series of thrust faults that strike NNE, S–N and NW. The Ludian syncline hosts the major orebodies, most of which outcrop along the two flanks of the syncline. The large orebodies were controlled by intersections of faults with NW and NE strikes (Fig. 1b).

The native copper mineralization is restricted to a transitional zone between the $P_2\beta_4$ unit and the Xuanwei Formation. The orebodies are hosted in volcanic breccias, welded tuffs and amygdaloidal basalts with pyroclastic features typical of volcanic vent environments, as well as carbonaceous–siliceous argillites typical of terrestrial sedimentation. Cu-sulfide and -oxide mineralization also can be seen, in some places, at the base of the $P_2\beta_4$ unit.

Exploration of native copper is being performed in the Ludian and Huize areas. Based on the estimation from surface exploration and mine, individual orebodies marked on Fig. 1a have Cu metal reserves of 20,000 to 60,000 t, with average grades of 3 to 10% Cu. Seven Cu-bearing layers, from bottom to top, are recognized in the Ludian syncline (Fig. 1b, c).

Layer 1: A tuffaceous layer with a thickness of about 10 m, containing Cu-oxide and -sulfide mineralization of low Cu grade (∼0.3 to 0.5 wt.%; sample M-3), which overlies the massive basalt bed of $P_2\beta_4$.

Layer 2: A pyrobitumen-bearing tuffaceous layer with a thickness of 1 to 2 m which hosts an orebody with a grade of 5 to 20 wt.% Cu (sample M-4). It is composed of boudinaged and/or lensoid lumps of pyrobitumen containing net-veined and disseminated native copper as well as massive chalcocite.

Layer 3: An amygdaloidal basaltic layer with a thickness of about 20 to 40 m that contains fine-grained and disseminated native copper and has a Cu grade of 0.1 to 14% (samples M-5 to M-8 and LD-7).

Layer 4: A welded tuff layer with a thickness of about 20 to 40 m, containing a heterogeneous mineralization zone which consists of disseminated and fine-grained native copper ranging in size from several μm to several mm (sample LD-14).

Layer 5: A carbonaceous–siliceous argillite layer with a thickness of 1 to 2 m is the second major lode of native copper. This takes the form of stockworks and disseminations of native copper (Cu grade: 10 to 15 wt. %; sample LD-5, LD-8-2 and LD-13).

Layer 6: A bituminous volcanic breccia layer with a thickness of 1 to 3 m contains picritic to andesitic debris in carbonaceous and/or siliceous cement. Mineralization consisting of native copper and tenorite with Cu grades varying from 0.3 to 20% is found within this layer. Some large pieces of flaky native copper ($30 \times 10 \times 0.2$ cm in size) fill cracks in this layer.

Layer 7: A siliceous–sandstone layer with a thickness ranging from 0 to 3 m at the base of the
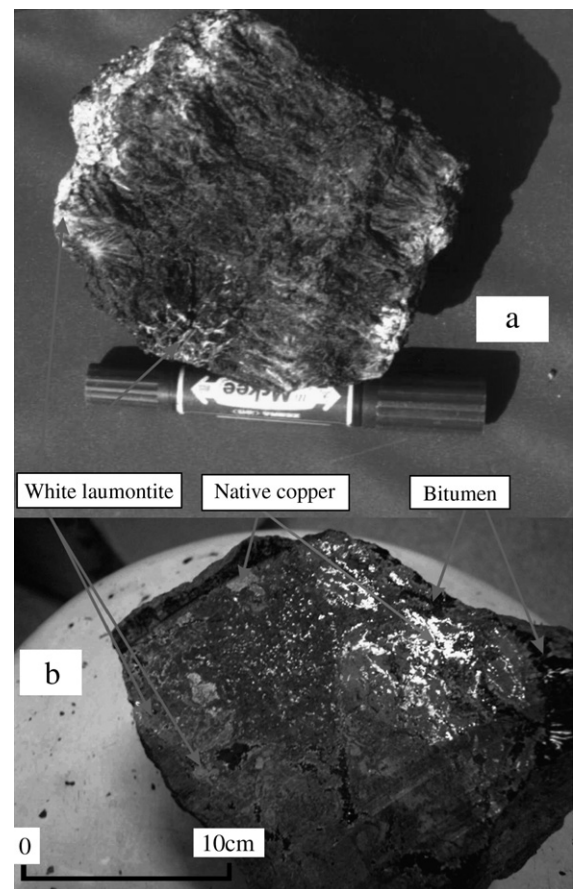

Fig. 2. Two photographs showing laumontite and native copper associations in a tuffaceous ore specimen from the Ludian syncline.

Xuanwei Formation; coal or clay are interbedded. The layer contains weak mineralization of disseminated native copper, tenorite, malachite and chalcocite.

Hydrothermal alteration of these rocks includes (from high to low temperature), actinolitization–magnetization–silicification, chloritization, bituminization, zeolitization and silicification–carbonation. No zoning of alteration mineralogy was observed.

Actinolitization–magnetitization–silicification consists of tremolite and/or actinolite form chrysanthemum-shaped or fibrous aggregates in carbonaceous–siliceous argillites and tuffaceous rocks with tenorite and a small amount of silica-copper minerals and native copper. The intensity of native copper mineralization decreases with increasing amounts of actinolite.

Chloritization: Chlorite can be seen in the pores of vesicular lavas and breccias; some are intergrowth with zeolites and weak native copper mineralization.

Bituminization: Fine-grained, lensoid and veined bitumens containing grains of native copper are found in cracks and pores of vesicular lavas, welded tuffs, volcanic breccias and carbonaceous argillites. These ores usually have a high Cu grade (>8%). Most of the bitumens have a light gray or brown color and mosaic coking or flux textures under reflected light microscope. They cannot be dissolved in CS_2 and thus having the properties of pyrobitumen (Jacob, 1989).

Zeolitization: Laumontites and heulandites are found in amygdaloidal basalts, volcanic breccias and welded tuffs. White laumontites are associated with disseminated native copper and copper oxide, which formed at an early stage. High-grade Cu ores are associated with laumontitization (Fig. 2). Brownish red heulandites with in disseminations, veins and vugs are associated with flaky native copper, and crosscut the disseminated copper ores.

Silicification: Siliceous rocks on top of the volcanic breccia layer have SiO_2 contents of up to 80 to 95 wt.%. Some siliceous rocks are high-grade ores containing stockwork and flaky native copper and tenorite, which are usually accompanied by bituminization. Intensity of copper mineralization increases with increasing silicification.

Carbonatization: Veinlet and granular carbonate and quartz fill vesicles and fractures in breccias and tuffaceous rocks and are associated with malachite, chalcocite and chalcopyrite.

3. Analytical methods

Ores and host rocks collected from a section crossing the Ludian syncline (Fig. 1b, c) were broken into cm-size chips. Fresh chips were selected and pulverized for chemical analysis. Minerals including actinolite, laumontite, heulandite, bitumen, quartz and carbonate were separated from the high-grade ores for $^{40}Ar/^{39}Ar$ and oxygen isotope analyses, fluid inclusion studies and vitrinite reflectance measurements.

Major element contents were analyzed using wet chemical methods. The concentrations of trace elements were determined using an ELAN 6000 ICP-MS instrument with errors lower than 5%. Oxygen isotope analyses of actinolite, quartz and carbonates were carried out on a Delta Plus XL mass spectrometer. Bitumen and vitrinite reflectance ($R_0\%$) determinations for bituminization samples were performed on a Leitz MPV 3 microscope photometer. Fluid inclusion homogenization temperatures for carbonates were determined on a Fluid Inc. adapted USGS gas-flow heating–freezing stage.

Pure laumontites and heulandites for $^{40}Ar/^{39}Ar$ dating were packed into cubic shapes with pure aluminum foil and intercalated with the ZBH-25 biotite standard. The composite package was sealed in a quartz vial and wrapped with cadmium sheet, then placed in an aluminum cylinder. The aluminum cylinder with samples was irradiated in the H8 channel of the fast neutron reactor at the Chinese Academy of Atomic Energy with an integrated total flux of about 10^{18} n/cm^2. Samples were degassed at ~100 °C for 3h. Step-heating of samples was performed in an electron bombarded furnace with temperature controlling accuracy of ±10 °C for 30min per step. Ar isotopic analyses were performed on a VG MM-1200 mass spectrometer in static mode. Blank levels for ^{40}Ar and other Ar isotopes (39, 38, 37 and 36) are 10^{-15} and 10^{-17} mol, respectively. Measurement errors of $^{39}Ar/^{40}Ar$ and $^{36}Ar/^{40}Ar$ are lower than 0.1% for the integrated plateau steps. The intercalated standards with a mean age of 131.6 ± 0.3 Ma (Wang, 1983) yielded J factors as listed in Table 3. The Ca and K correction factors used are $(^{36}Ar/^{37}Ar)_{Ca}=2.64\times10^{-4}$, $(^{39}Ar/^{37}Ar)_{Ca}=6.87\times10^{-4}$ and $(^{40}Ar/^{39}Ar)_K=7.15\times10^{-3}$, respectively. Decay constants used in age calculations are those recommended by Steiger and Jager (1977).

Samples for analyses of U–Th–Pb isotopic systematics were dissolved with HF+HNO$_3$. Concentrations of U, Th and Pb were determined using quantitative analytical method on ICP-MS of ELAN 6000 with errors lower than 2%. Pb was extracted from other batch solutions in a micro-exchange column of anion resin of Dowex-I (200 to 400 mesh) in HBr solution. Pb isotopic ratio measurements were made on a VG-354 for with precisions of <0.07%

Table 1
Contents of copper, other major and trace elements, organic matter and lead isotope ratios in various ore types

No	M-8	M-5	M-6	M-3	M-4	LD-2	LD-3	LD-4	LD-5A	LD-5B	LD-6
Ore type	Breccia	Basalt	Basalt	Tuff	Silicalite	Breccia	Breccia	Breccia	Argillite	Argillite	Breccia
SiO_2	44.68	49.35	49.06	53.41	79.13	42.97	37.40	40.31	63.63	69.33	37.34
Al_2O_3	17.01	11.72	13.33	25.18	7.51	16.18	20.97	17.86	21.14	17.64	22.09
Fe_2O_3	6.16	9.79	7.63	2.62	1.54	4.24	6.26	2.12	1.00	0.19	7.00
FeO	10.07	6.17	5.64	6.87	4.46	16.73	16.95	15.78	1.65	1.50	12.49
MnO	0.23	0.20	0.18	0.11	0.09	0.30	0.45	0.31	0.04	0.03	0.40
MgO	9.82	5.63	5.32	2.09	0.88	9.02	8.51	8.74	0.16	0.12	4.97
CaO	3.19	5.95	6.38	2.55	3.56	3.56	3.25	6.70	10.35	7.48	7.25
Na_2O	0.78	7.18	7.39	1.45	1.27	0.69	0.21	0.58	0.21	2.07	0.61
K_2O	3.45	0.10	1.08	2.56	0.22	2.81	1.53	2.45	0.43	0.68	2.36
P_2O_5	0.24	0.42	0.53	0.60	0.42	0.22	0.30	1.37	0.19	0.51	0.08
Organic matter	1.45	0.08	0.08	1.19	34.64	3.0	3.4	0.14	10.35	10.65	0.99
Volatile	8.52	2.73	3.35	14.05	8.32	8.50	9.16	10.43	7.75	8.65	10.88
Cu	0.59	0.81	0.39	0.49	24.15	0.50	0.30	0.56	14.20	15.50	0.41
Sc	35.3	29.5	28.7	22.6	2.56	22.5	33.9	30.3	5.92	2.20	35.2
Ti	26,370	21,080	20,790	15,430	2077	19,680	27,850	22,680	7140	1740	31,320
V	427	400.2	399.1	129.6	57.1	453	463	417	133	193	524
Cr	46.2	38.2	37.7	21.15	6.67	33.5	44.79	40.1	12.1	6.17	52.2
Co	56.9	46.61	42.33	58.39	20.16	78.6	83.11	61.3	7.62	5.43	94.4
Ni	65.5	55.3	52.8	40.0	14.1	61.6	84	59.1	9.02	4.71	101
Zn	99.4	150.5	182	77.4	27.88	108	125.2	101	22.2	13.5	170
Ga	22.8	26.35	17.7	44.0	10.86	34.1	32.85	25.8	12.1	7.54	30.5
Ge	1.11	2.187	1.69	1.56	1.057	2.46	1.361	1.67	0.45	0.48	1.13
Rb	150	2.41	4.31	108	9.13	53.3	71.9	58.3	8.37	16.9	79.7
Sr	104	105.9	348	296	194.9	211	184	190	288	241	138
Y	32.8	33.85	33.5	104	34.27	42.2	73.6	70.1	17.1	14.3	74.8
Zr	350	278	269	1133	189	314	524	357	118	37.0	694
Nb	43.5	34.5	34.0	126	28.1	42.6	64.7	48.3	15.8	5.44	76.9
Ba	766	54.7	102	833	104	1938	1115	2027	98.7	190	477
La	33.5	32.4	48.2	113	35.4	32.3	63.3	85.0	13.4	7.69	65.3
Ce	83.3	74.1	94.2	261	87.9	89.3	127	222	31.0	29.8	125
Pr	11.4	10.1	12.1	36.2	13.7	16.8	18.9	38.4	4.89	6.36	16.5
Nd	47.2	43.1	51.1	144	58.0	78.2	77.3	183	23.1	37.0	64.1
Sm	9.95	8.79	10.4	28.8	11.3	16.9	15.4	35.6	4.48	9.41	14.5
Eu	2.99	2.77	3.12	6.57	2.71	5.51	4.97	11.6	0.96	1.76	4.03
Gd	8.93	8.00	9.08	25.7	9.10	14.0	16.35	30.1	3.96	6.86	16.0
Tb	1.44	1.23	1.26	4.01	1.36	1.91	2.58	3.57	0.56	0.72	2.64
Dy	8.39	6.89	6.79	23.8	7.23	9.74	15.7	15.8	3.00	2.78	15.4
Ho	1.53	1.24	1.24	4.42	1.23	1.69	3.08	2.59	0.57	0.38	2.93
Er	3.97	3.18	3.17	12.0	3.02	4.53	8.31	6.26	1.46	0.82	7.44
Tm	0.56	0.44	0.43	1.78	0.39	0.67	1.2	0.79	0.20	0.09	1.09
Yb	3.49	2.86	2.78	11.0	2.18	4.28	7.17	4.77	1.29	0.54	6.88
Lu	0.53	0.44	0.43	1.67	0.32	0.65	1.14	0.71	0.19	0.08	1.05
Hf	10.3	7.68	7.36	28.6	4.01	9.66	16.0	10.7	3.37	1.31	17.0
Ta	3.33	2.67	2.58	8.52	2.45	3.98	4.91	3.92	1.26	0.57	5.42
Pb	7.35	5.474	5.04	5.80	1.01	5.54	7.63	7.31	2.85	1.37	15.6
Th	7.48	5.432	5.30	27.2	3.26	7.66	14.5	8.32	2.92	0.85	15.4
U	2.01	1.23	1.14	4.74	0.76	8.77	2.87	2.82	0.56	0.26	2.77
$^{238}U/^{204}Pb$		14.55		54.44		105.1	24.44				11.60
$^{232}Th/^{204}Pb$		65.90		319.9		94.17	126.6				66.28
$^{206}Pb/^{204}Pb$		18.818		19.582		20.843	18.905				18.819
$^{207}Pb/^{204}Pb$		15.529		15.572		15.549	15.488				15.614
$^{208}Pb/^{204}Pb$		38.978		40.546		38.869	39.225				39.343

*Contents for major elements and Cu are %, concentrations for trace elements are ppm. The major element data are normalized to 100% on a volatile-free basis.

LD-7 Basalt	LD-8 Breccia	LD-10 Breccia	LD-11A Breccia	LD-11B Breccia	LD-12 Breccia	LD-14 Tuff	LD-41 Breccia	LD-8-2 Silicalite	LD-13 Silicalite	M-7 Silicalite
48.19	44.55	41.88	37.81	40.05	54.28	61.42	39.98	95.02	94.22	74.39
15.85	21.31	18.69	20.39	20.57	15.14	15.37	20.78	1.33	1.75	8.07
11.16	1.25	1.33	1.72	1.30	0.50	0.48	8.17	0.31	0.22	3.40
4.15	12.49	11.32	14.60	12.72	8.33	3.21	11.37	0.84	0.63	1.27
0.15	0.22	0.27	0.34	0.29	0.16	0.07	0.37	0.01	0.01	0.10
2.14	6.66	9.78	10.61	10.35	8.74	1.44	4.22	0.03	0.94	0.08
15.84	8.81	10.55	7.98	7.57	4.42	14.53	4.26	1.61	1.93	10.11
0.05	0.28	0.66	0.23	0.09	1.15	1.23	1.25	0.60	0.05	0.94
0.02	0.90	0.94	1.94	2.43	2.75	0.39	2.78	0.03	0.01	0.14
0.34	0.52	0.13	0.09	0.07	0.57	0.10	2.32	0.05	/	0.61
3.54			0.60	0.59		3.33		7.92	7.60	3.49
3.14	14.00	12.97	11.00	10.95	9.83	10.08	10.80	3.21	1.74	0.85
5.21	0.29	0.64	0.65	0.64	3.20	3.47	0.54	12.64	2.59	0.64
26.76	25.34	32.3	32.0	33.0	29.3	13.79	35.3	0.53	0.55	9.38
12,570	19,750	26,760	25,680	27,360	23,760	11,480	27,060	1020	1260	5340
381	322	409	416	397	616	208	424	74.1	39.6	56.0
42.4	33.17	43.7	39.5	42.8	43.8	21.29	48.8	5.38	5.74	12.9
50.2	48.4	47.2	59.5	51.4	35.9	14.9	85.9	0.28	0.49	3.01
53.5	60.7	58.3	79.5	67.8	44.4	19.0	80.1	1.97	2.05	10.9
57.7	91.0	126	148	134	93.2	42.3	176	11.2	7.86	17.5
86.0	28	27.8	33.4	32.1	23.2	14.5	27.8	0.52	0.45	15.6
13.9	1.86	1.70	1.67	1.53	2.73	1.21	1.23	0.46	0.52	7.01
0.29	36.2	37.8	64.3	80.4	64.3	10.9	66.8	0.44	0.28	1.29
66.0	353	182	87.0	102	114	326	197	17.8	13.3	2934
28.1	77.3	82.0	74.7	75.2	49.2	33.3	79.2	2.56	3.19	42.4
146	404	576	521	536	359	243	319	9.39	17.6	266
18.1	50.4	78.8	73.9	76.7	49.4	28.4	42.4	0.98	1.81	35.4
16.5	267	217	318	446	1082	199	2161	17.6	19.7	833
62.9	44.9	17.3	35.8	35.1	43.2	52.2	108.5	0.48	0.60	57.1
105.1	129	45.9	116	110	116	127	276	2.44	3.25	88.0
10.2	25.8	7.97	20.2	18.3	17.4	19.2	41.4	0.52	0.69	12.5
37.6	116	34.2	88.6	75.1	72.5	83.9	195	2.33	3.31	50.0
6.80	24.5	7.58	20.7	15.8	14.8	16.5	38.9	0.53	0.65	8.74
2.25	6.82	2.15	5.60	4.59	4.62	4.56	10.8	0.11	0.13	2.30
6.17	21.8	6.88	19.3	16.2	15.9	14.7	32.0	0.46	0.62	8.26
0.891	2.98	1.12	3.38	2.95	2.81	2.16	3.81	0.075	0.09	1.32
5.15	16.0	6.76	18.8	16.7	16.4	11.4	16.4	0.43	0.52	7.27
0.95	2.89	1.32	3.40	3.03	3.02	2.07	2.65	0.083	0.1	1.40
2.49	7.26	3.62	8.29	7.57	7.49	5.04	6.20	0.21	0.27	3.58
0.34	0.99	0.53	1.18	1.04	1.00	0.70	0.79	0.031	0.04	0.52
2.24	5.85	3.17	7.02	6.12	5.92	4.28	4.68	0.183	0.22	3.09
0.35	0.86	0.49	1.04	0.90	0.86	0.62	0.68	0.034	0.03	0.47
3.98	11.5	15.1	14.0	14.5	9.48	6.56	8.38	0.026	0.37	6.29
1.49	3.72	5.44	5.12	5.32	3.40	1.98	3.01	0.039	0.10	2.06
2.66	3.10	4.82	5.30	5.03	5.22	2.67	9.71	0.55	1.88	11.4
2.85	11.1	14.7	13.5	13.5	8.33	6.18	6.47	0.099	0.18	6.02
0.60	1.95	2.50	2.35	2.36	5.03	1.26	1.97	0.11	0.11	0.83
	41.42	34.13			63.41	30.89			3.77	
	242.3	206.0			107.7	155.5			6.33	
	19.173	19.152			19.814	19.121			18.582	
	15.579	15.559			15.564	15.613			15.661	
	39.865	39.867			39.202	39.454			38.788	

Table 2
Geochemical data for temperature estimation of hydrothermal fluids

	Metasomatized mineral association* and temperature ranges	Bitumen $R_0\%$	T (°C) calculated from $R_0\%$	Th (°C) of inclusions in carbonates	Mineral $\delta^{18}O_{smow}$(‰)	Fluid temperature and $\delta^{18}O(H_2O)$ calculated from mineral $\delta^{18}O$
M-4	Act., Q., Lau., Bit. Ncu., Chal. (420–100 °C)	1.62 ± 0.06	215		Act.16.0, Q. 22.9	T=370 ± 20 °C $\delta^{18}O$=16.8 ± 1.0
LD-8	Act., Lau., Bit., Heu., Ncu. (420–100 °C)	1.55 ± 0.10	210			
DD-1, -2, -3	Lau., Bit., Heu., Ca., Ncu (350–100 °C)	1.65 ± 0.02	218	197–224, 162–170, 103–150	Ca. 19.2, 19.1, 17.6	
SJQ-1	Bit., Heu., Ca., Ncu (220–100 °C)	1.80 ± 0.03	229	108–139	Ca.12.2, Q. 15.6	T=180 ± 10 °C $\delta^{18}O$=0.8 ± 0.2
SJQ-2	Lau., Bit., Heu., Ca., Ncu (350–100 °C)	1.83 ± 0.07	231			
LG-3	Bit., Heu., Ca., Ncu (220–100 °C)	1.61 ± 0.09	215			

*Mineral abbreviations: Act—actinolite; Q—Quartz; Lau—laumontite; Bit—bitumen; Heu—heulandite; Ca—carbonate; Chal—chalcocite, Ncu—native copper.

Table 3
$^{40}Ar/^{39}Ar$ data of step-heating for zeolite samples undisturbed by chlorine

T ($C°$)	$^{36}Ar/^{40}Ar$	$^{39}Ar/^{40}Ar$	$^{40}Ar*/^{39}Ar_K$	total ^{39}Ar (10^{-12} mol)	^{39}Ar (%)	$^{40}Ar*$ (%)	Age (Ma)	1σ	Ca/K	Cl/K
LD-14-3 Laumontite 0.2886 g J = 0.0040754										
500	0.002260	0.009896	33.56	0.005	1.87	35.26	231.2	13.8	4.56	0.0385
650	0.001741	0.017846	27.20	0.025	8.95	48.56	187.4	1.9	2.04	0.0242
750	0.001651	0.015443	33.17	0.052	18.89	51.23	228.5	2.3	1.42	0.00947
850	0.001582	0.016441	32.38	0.069	24.6	53.25	223.1	1.5	1.41	0.00752
1000	0.001549	0.016146	33.59	0.085	30.28	54.24	231.4	3.0	1.41	0.00363
1100	0.001621	0.01564	33.31	0.043	15.24	52.13	229.5	4.6	2.93	0.00353
1200	0.001659	0.015192	33.56	0.001	0.52	51.56	231.1	46.5	47.6	0.215
YSD-1 Laumontite 0.3212 g J = 0.0040798										
500	0.001887	0.01257	35.20	0.027	2.24	44.25	242.7	6.0	6.19	0.185
690	0.001619	0.02222	23.47	0.093	7.59	52.15	161.9	0.7	3.91	0.112
800	0.001475	0.01936	29.13	0.130	10.86	56.41	200.9	0.8	4.04	0.0797
950	0.001401	0.01812	32.35	0.251	20.50	58.61	223.1	0.4	2.74	0.0399
1050	0.001278	0.01840	33.84	0.383	31.24	62.24	233.3	0.5	2.21	0.0176
1150	0.001093	0.02018	33.55	0.208	17.00	63.13	231.3	0.9	4.26	0.0173
1250	0.001397	0.01704	34.45	0.104	8.47	60.16	237.8	2.4	4.74	0.0313
1350	0.001753	0.01376	35.03	0.029	2.34	52.47	241.5	2.5	16.5	0.162
YC-1 Laumontite 0.5524 g J = 0.0040776										
500	0.002031	0.01192	32.55	0.004	1.28	37.19	231.4	29.1	5.91	0.0721
650	0.002049	0.01465	26.84	0.032	9.54	39.46	185.7	2.4	1.70	0.0316
750	0.001777	0.01622	29.22	0.078	23.47	47.50	201.9	1.4	1.02	0.0255
850	0.001728	0.01470	33.24	0.097	28.64	48.93	229.6	0.9	0.905	0.0271
1000	0.001672	0.01542	32.76	0.102	30.04	50.60	226.3	1.5	0.983	0.0229
1080	0.001652	0.01502	33.76	0.020	5.78	51.25	235.9	10.5	6.08	0.144
1200	0.001433	0.01741	32.35	0.005	1.55	50.36	228.4	33.5	14.1	0.457
LG-2 Heulandite 0.4937 g J = 0.0040732										
350	0.002287	0.01106	29.31	0.014	2.41	32.42	202.2	8.2	1.40	0.0319
500	0.001853	0.02311	19.58	0.057	9.47	45.25	135.0	1.0	1.03	0.0178
650	0.001728	0.02553	19.17	0.129	21.91	48.94	132.2	0.7	0.625	0.0122
750	0.001739	0.02467	19.70	0.182	30.28	48.60	135.9	0.4	0.477	0.0095
850	0.001571	0.02778	19.29	0.164	27.32	53.60	133.0	0.9	0.716	0.0147
1000	0.001678	0.02430	20.74	0.040	6.58	51.15	143.1	4.2	2.86	0.0578
1200	0.001617	0.01695	30.82	0.015	2.56	52.27	212.6	7.9	4.13	0.0848

(2σ). The mean measured value for standard SRM-981 is $^{206}Pb/^{204}Pb = 16.934 \pm 0.007$, $^{207}Pb/^{204}Pb = 15.486 \pm 0.012$ and $^{208}Pb/^{204}Pb = 36.673 \pm 0.033$, which are in good agreement with the recalibrated values of double-spike determination: 16.9322, 15.4855, and 36.6856, respectively (Todt et al., 1993).

4. Results and discussion

Major and trace element, organic matter and copper contents for 22 ore samples are listed in Table 1. The analytical data for bitumen $R_0\%$, $\delta^{18}O_{smow}$ of alteration minerals (actinolite, quartz and carbonate) and Th°C of inclusions in carbonates are given in Table 2. $^{40}Ar/^{39}Ar$ step-heating data for four zeolite samples are given in Table 3. The analytical results for U–Th–Pb isotopic systematics are listed in Table 1.

4.1. Geochemical evidence for hydrothermal mineralization

REE concentrations in ores show large variations ($\Sigma REE = 8-738$ ppm) increasing from silicate and argillite ores (8 to 207 ppm) to CFB host rocks (200–290 ppm) (Zhu et al., 2005a) to breccia and tuff ores (217 to 738 ppm). REE patterns and a Ce/Pr–Eu/Eu* diagram normalized to chondrite show Eu and La–Ce negative anomalies for most of the ores (Figs. 3 and 4a). These features are clearly related to hydrothermal fluids containing halogen complexes at moderately high temperatures (Haas et al., 1995; Whitney and Olmsted, 1998; Smith et al., 2000; Allen and Seyfried, 2005). Lack of a positive Eu anomaly is generally associated with reducing conditions, which favors Eu^{2+}. There is an inverse correlation between Eu/Eu*–HREE (Yb) for breccia ores, whereas there is a positive correlation for silicate–argillite ores (Fig. 4b).

Variations in the concentration of HFSE (Zr, Nb, Hf, Ta and Th) in ores are also larger than those of the CFB host rocks. Zr–Nb, Hf–Ta and Hf–Th plots show positive correlations (Fig. 5). Zr(Hf) and Nb(Ta,Th) have very different solid–liquid bulk partition in an upper mantle melting regime, and therefore it is difficult to account for these linear correlations by partial melting or fractional crystallization of mafic magmas (Kamer and Collerson, 2000). However, these elements have similar chemical
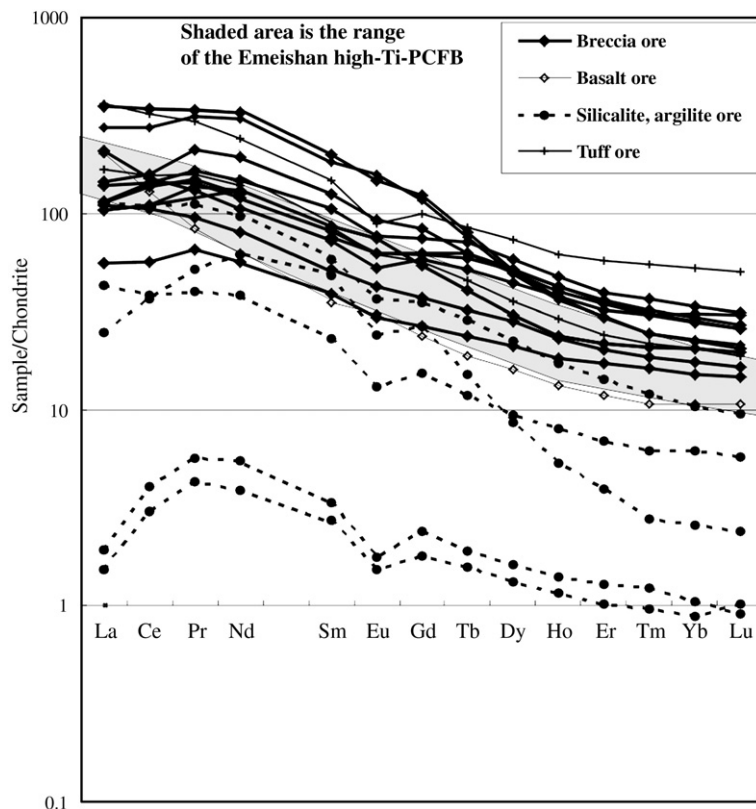
Fig. 3. Chondrite-normalized REE patterns for ores.
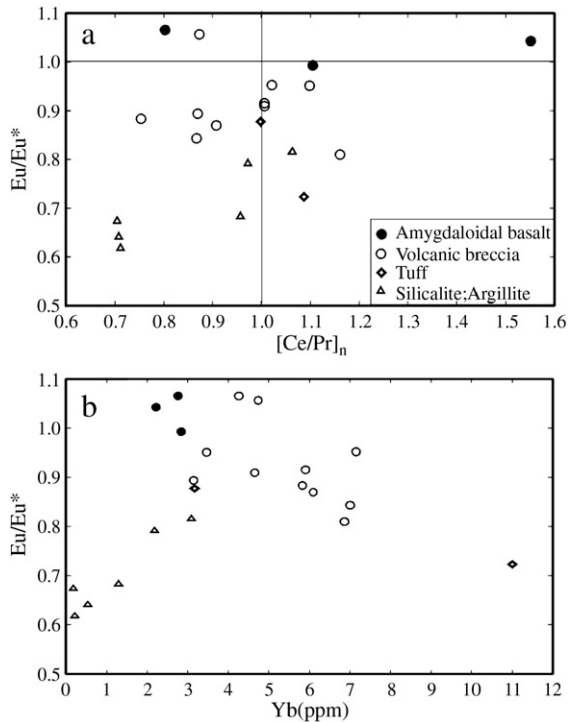
Fig. 4. Chondrite-normalized Ce/Pr–Eu/Eu*(a) and Yb–Eu/Eu*(b) plots for ores.

properties in halogen or carbonate complexes in alkaline aqueous fluids. Precipitation of these elements during hydrothermal metasomatism is controlled by temperature, as well as halogen, K_2O+Na_2O and Al_2O_3 contents (Hole et al., 1992; Aja et al., 1995; Jiang, 2000; Jiang et al., 2003). Hydrothermal metasomatism also yielded positive correlations between HSFE–HREE, Ti–V and Ti–Zr. The positive correlations between native copper grades and SiO_2 and bitumen contents indicate that Cu was transported in siliceous fluids and precipitated as native copper by reduction caused by reaction with bitumen.

4.2. Temperature constraints

The mineral association derived from hydrothermal metasomatism shows the following sequence from moderate to low temperatures: actinolite, chlorite, magnetite, laumontite, bitumen, quartz, native copper, heulandite, carbonate, siderite and chalcocite (Table 2). Actinolite forms at a temperature of ca. 400 to 420 °C (Sueno et al., 1973; Jenkins and Bozhilov, 2003). Laumontite has a temperature range of phase stability of 170 to 350 °C (Carlos and Bradley, 1997). The formation temperature of heulandite coexisting with carbonates is lower than 200 °C (Carr et al., 1999). Chalcocite usually crystallizes at a temperature lower

than 105 °C (Hamilton, 1967). Determination of oxygen isotopes yields $\delta^{18}O_{smow}$ of 16.0 and 22.9 for actinolite and quartz respectively and a fluid temperature of 370 ± 20 °C and $\delta^{18}O_{smow}(H_2O)=16.8\pm1.0$ (Table 2) (Zheng, 1993). Bitumenization took place after the actinolitization, but slightly earlier than deposition of the native copper mineralization. Determination of vitrinite reflectance $R_0\%$ for the bitumen from various ores shows a range of 1.55 to 1.83, indicating a temperature range of 210 to 230 °C (Table 2) (Barker and Pawlewicz, 1986). Carbonatization was usually later
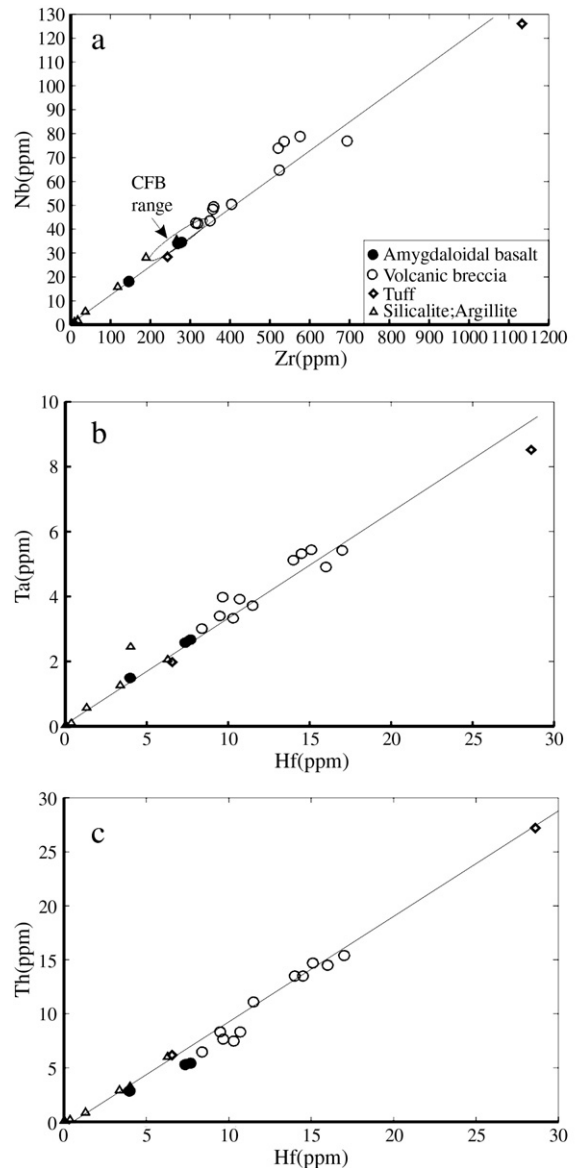
Fig. 5. Zr–Nb(a), Hf–Ta(b) and Hf–Th(c) correlation diagram for ores.

than deposition of native copper. Homogeneous temperature determinations of liquid inclusions for calcites from the DD (Dadi) and SJQ (Sujiaqing) orebodies yield temperature ranges of 197 to 224 °C and 103 to 170 °C, respectively (Table 2), indicating a temperature range of

about 200 to 210 °C for native copper. Oxygen isotopes in tuffaceous ores yield $\delta^{18}O_{smow}$ of 12.2 and 15.6 for calcite and quartz, respectively, which gives a fluid temperature of 180 ± 10 °C and $\delta^{18}O_{smow}(H_2O) = 0.8 \pm 0.2$ according to the geothermometric equations of Zheng (1993).
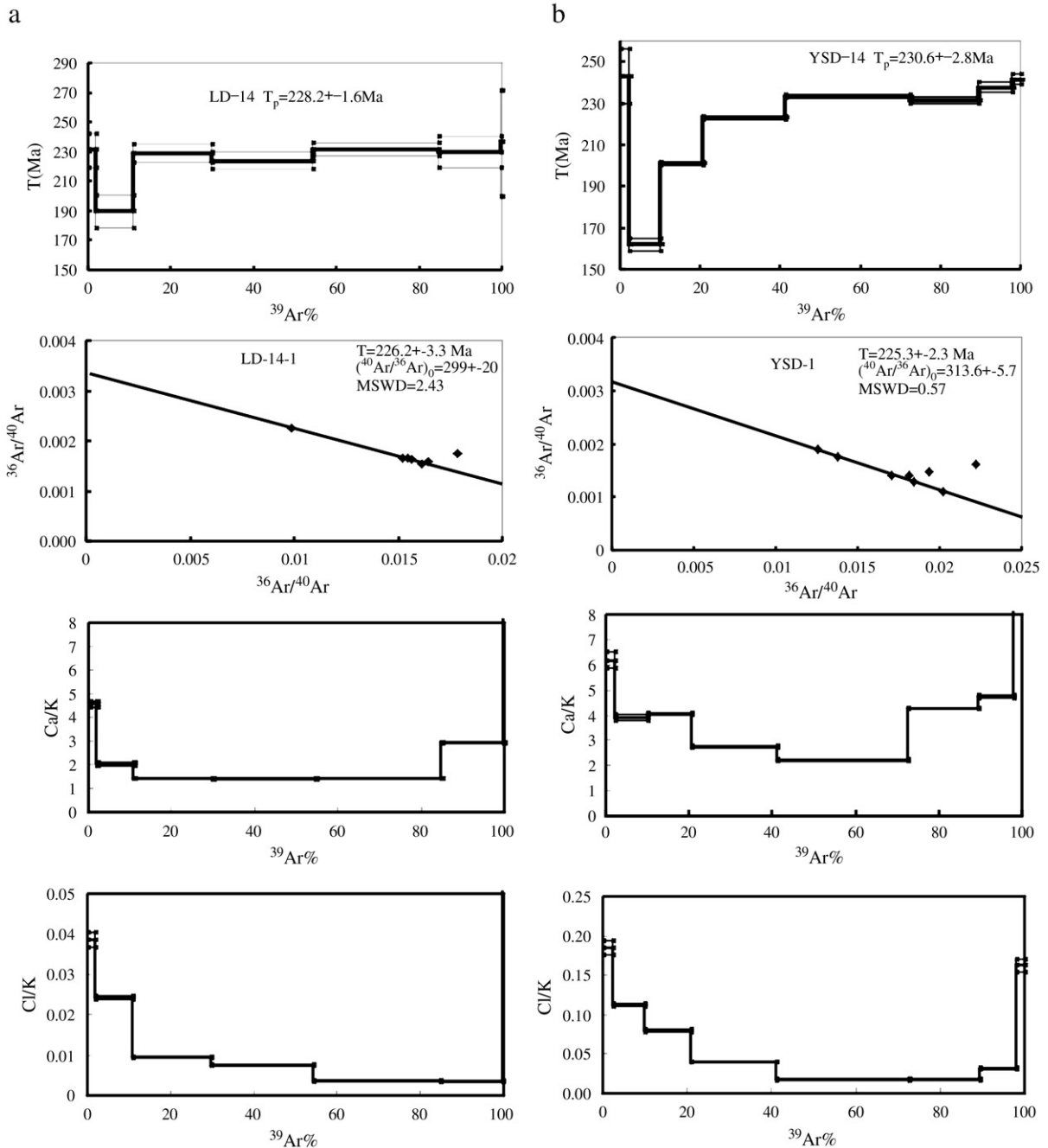
Fig. 6. $^{40}Ar/^{39}Ar$ age, Ca/K and Cl/K spectra and $^{36}Ar/^{40}Ar$–$^{39}Ar/^{40}Ar$ inverse isochrons for laumontite and heulandite samples. (a). LD-14-3 laumontite from the Ludian syncline; (b). YSD-1 laumontite from the Maoling syncline; (c). YC-1 laumontite from the Yiche syncline; (d). LG-2 heulandite from the Ludian syncline.
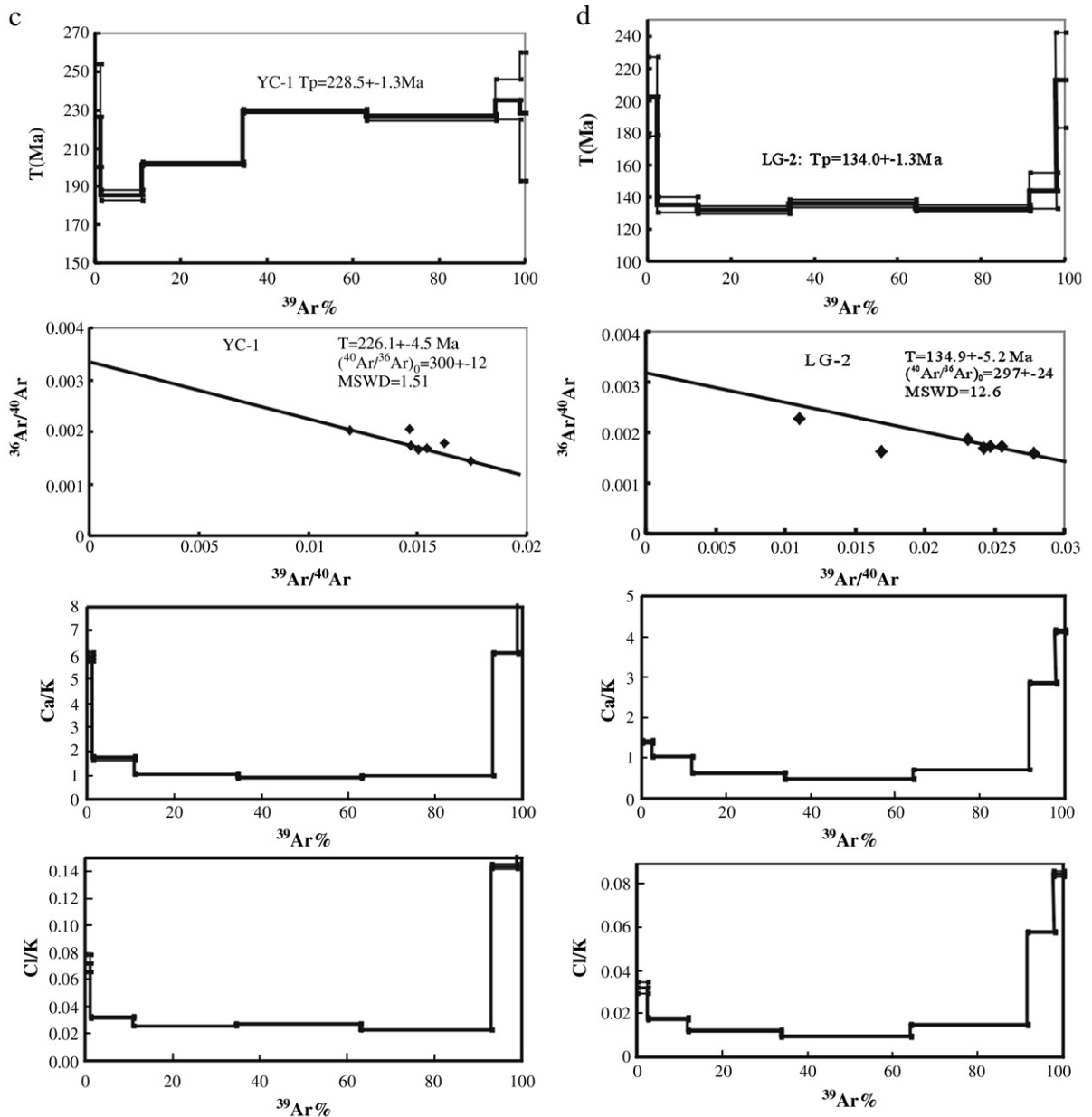
Fig. 6 (continued).

4.3. Geochronological constraints

4.3.1. Laumontite ^{40}Ar/^{39}Ar dating

Laumontite samples (LD-14-3, YSD-1 and YC-1) from three synclines show similar ^{40}Ar/^{39} age spectra; there are steps of age decreasing with V-shape at temperatures between 600 °C–800 °C and stable age plateaus with consistent ages occur at temperatures only above 800 °C. Based on the χ^2 test, integrated plateaus with 4 to 6 steps are recognized. Integrated

plateau ages are calculated according to ^{39}Ar release weight. Ages at the first steps (450 to 500 °C) are usually comparable with the plateau ages (Fig. 6). The LD-14-3 laumontite yields an integrated plateau age of 228.2±1.6 Ma, accounting for 5 steps and 89% ^{39}Ar release. Its ^{36}Ar/^{40}Ar–^{39}Ar/^{40}Ar inverse isochron age calculated on the integrated plateau and first steps is 226.2±3.3 Ma with MSWD=2.43 and (^{40}Ar/^{36}Ar)$_0$=299.4. YSD-1 gives an integrated plateau age of 230.6±2.8 Ma accounting for 6 steps and

77.2% ^{39}Ar release. The corresponding inverse isochron yields an intercept age of 225.3 ± 2.3 Ma with MSWD $= 0.57$ and $(^{40}Ar/^{36}Ar)_0 = 313.6$. YC-1 gives an integrated plateau age of 228.5 ± 1.3 Ma and an isochron age of 226.1 ± 4.5 Ma with MSWD $= 1.51$ and $(^{40}Ar/^{36}Ar)_0 = 300.3$ in 4 steps and 66% ^{39}Ar release. Although the three samples were collected from different orebodies, separated by a distance of 120 km, they show consistent plateau and isochron ages within deviation ranges.

As the initial $(^{40}Ar/^{36}Ar)_0$ ratios are slightly higher than those of air argon, a small amount of excess argon may have been present in the samples. The Ca/K and Cl/K spectra (Fig. 6) for the three samples indicate that the integrated plateaus occur at the steps with low Ca/K and Cl/K ratios. The revised amounts for ^{36}Ar and ^{39}Ar derived from calcium irradiation for the integrated plateau steps are lower than 0.4 and 0.1%, respectively. The Cl/K ratios are lower than 0.02 for the integrated plateau steps. The neutron-induced production of ^{36}Ar due to Cl only accounts for 10^{-5} of ^{36}Ar, and cosmic ray-produced ^{36}Ar during 230 My is lower than 10^{-15} g/g in the samples, so that chlorine corrections are not important. Therefore, the $^{40}Ar/^{39}Ar$ ages of laumontites (226 to 228 Ma) are considered to be reliable.

4.3.2. Heulandite $^{40}Ar/^{39}Ar$ dating

^{39}Ar release of 88.5% at temperatures from 500 to 1000 °C in 5 heating steps for the LG-2 heulandite yields a flat plateau age of 134.0 ± 1.7 Ma. The $^{40}Ar/^{39}Ar$ ages at steps of <500 and >1000 °C are close to the plateau ages of the laumontite samples. As argon release quantities in each step are similar, the variation range of $^{36}Ar/^{40}Ar$ and $^{39}Ar/^{40}Ar$ data is very small. Thus its isochron age (134.9 ± 5.2 Ma) and initial $(^{40}Ar/^{36}Ar)_0$ (297.0) show large deviation. The Ca/K and Cl/K spectra indicate that the revised amounts for ^{36}Ar and ^{39}Ar are quite low (<0.1%).

4.3.3. U–Th–Pb isotopic systematics

U, Th and Pb concentrations in the bituminized ores vary from 0.1 to 8.8 ppm, 0.2 to 27 ppm and 1.9 to 15.5 ppm, respectively, indicating no significant enrichment. However, $^{238}U/^{204}Pb(\mu$ value) and $^{232}Th/^{204}Pb$ ratios show wider ranges from 3.8 to 105 and 6.3 to 320, respectively, which are thus suitable for U–Pb and Th–Pb isochron dating. A μ-$^{206}Pb/^{204}Pb$ plot shows a good linear correlation and yields a U–Pb isochron age of 136 ± 11 Ma (Fig. 7), in agreement with the $^{40}Ar/^{39}Ar$ plateau and isochron ages of LG-2 heulandite. There is also a $^{232}Th/^{204}Pb$–$^{208}Pb/^{204}Pb$ isochron indicating an

age of about 129 ± 18 Ma for all data except LD-6 and LD-13. However, there is no linear correlation between $^{206}Pb/^{204}Pb$ and $^{207}Pb/^{204}Pb$.

4.4. Genesis of native copper mineralization

The High Ti–P CFB, which erupted during the Late Permian in northeastern Yunnan, produced rocks with high background Cu content (mean 207 ppm). Early hydrothermal processes formed magnetite and actinolite at temperatures of about 400 to 420 °C. Precipitation of magnetite caused a decrease in concentrations of REE and HFSE, an increase in Eu/Eu* and reducibility of the hydrothermal fluids (Fig. 4), which were associated with weak native copper and copper oxide mineralization. Laumontites filled fractures in breccias and tuffs and was associated with native copper and bitumen. Bituminization provided a reducing environment, which encouraged precipitation of native copper. As laumontites have a temperature range of phase stability of 170 to 350 °C (Carlos and Bradley, 1997), comparable with that of bitumen formation (210 to 230 °C), their $^{40}Ar/^{39}Ar$ ages (226 to 228 Ma) represent a first stage of native copper mineralization. An important zone of Pb–Zn–Ag–Ge mineralization strikes NNE, approximately parallel with that of native copper mineralization (Fig. 1a). These deposits are hosted in strata of Lower Permian to Devonian age, show veined-, bag- or cylinder-like
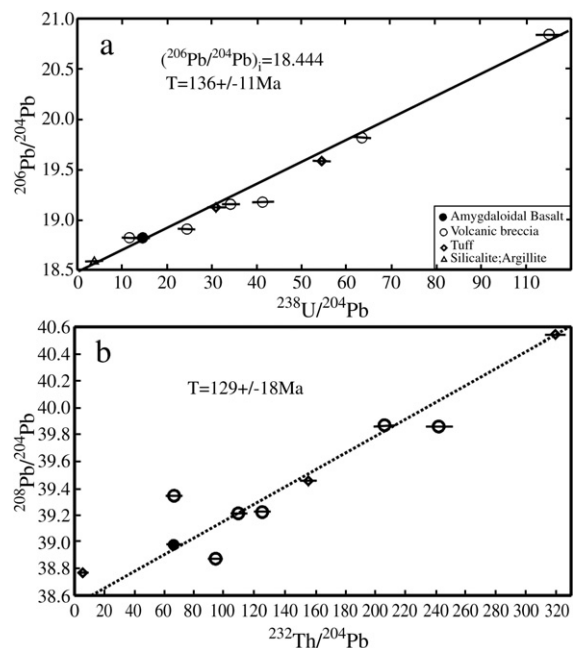

Fig. 7. (a) μ-$^{206}Pb/^{204}Pb$–$^{238}U/^{204}Pb$ and (b) $^{232}Th/^{204}Pb$–$^{208}Pb/^{204}Pb$ isochron diagrams for bituminized copper ores.
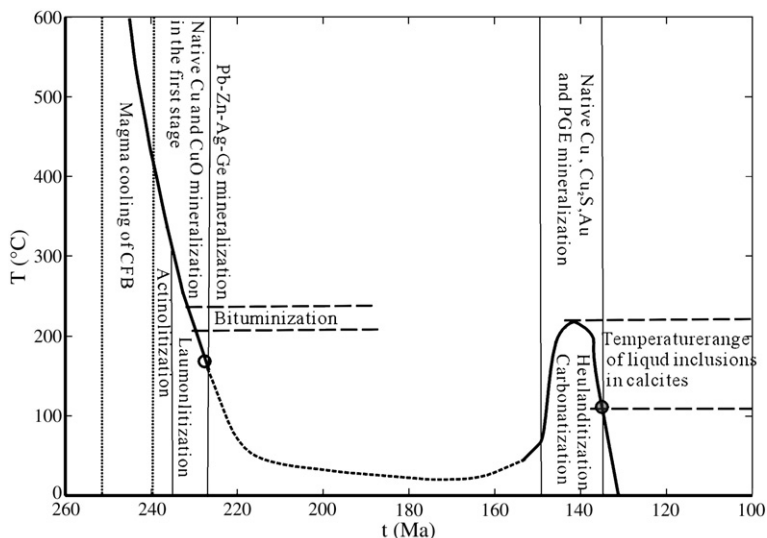
Fig. 8. T(temperature)$-t$(time) diagram for two-stage native copper mineralization in the Emeishan CFB, northeastern Yunnan.

morphologies and are controlled by faults of NW strike. Two superlarge, three large and two medium deposits with total reserves of about 8 Mt (Zn+Pb metal) and high-grade (>20%) have been confirmed by exploration. Based on the Sm–Nd isochron age (225±15 Ma) of carbonates and the Rb–Sr isochron age (225.6±3.1 Ma) of sphalerites published by Huang et al. (2005), the Pb–Zn–Ag–Ge deposits in this area have the same age (225 to 226 Ma) as the native copper deposits. Therefore, intense hydrothermal activity followed the Emeishan CFB eruption in northeastern Yunnan. The time interval between termination of basalt eruption and large-scale mineralization in the Ludian area was about 15 to 20 Ma, which is comparable to that of the Keweenawan native copper deposit in Michigan (~20 Ma; Bornhorst et al., 1988; Davis and Paces, 1990). Although late dikes or intrusions with ages of 220 to 230 Ma are not found in this area, shallow magma chambers or hot intrusive bodies beneath the eruption channel might have persisted for about 15 to 20 Ma and provided heat for hydrothermal activity.

Fluid inclusion temperature indicate that carbonatization developed at temperatures of about 100 to 220 °C. Magnetites have been altered into siderites at a reducing environment induced by bituminization, which affected remigration and repartition of REE, HFSE and U–Th–Pb isotopic systematics in the breccias and tuffs. Formation temperatures of heulandite, less than 200 °C, were similar. The LG-2 heulandite yields a stable ^{40}Ar/^{39}Ar plateau age of 134 Ma. Based on the ^{39}Ar release pattern of this sample, its closure tem-

perature T_b can be estimated to be about 70 to 100 °C (McDougall and Harrison, 1988). Therefore, this may represent a cooling age related to regional uplifting or another hydrothermal event related to native copper mineralization. As the U–Pb isochron age of breccia ores (136 Ma) is in agreement with the ^{40}Ar/^{39}Ar age of LG-2 heulandite, this indicates a period of U–Th–Pb migration and possible second stage native copper mineralization during the Early Cretaceous. A regional uplift and extension event associated with mafic dike intrusions in eastern Yunnan and western Guizhou during the Late Jurassic (133 Ma) has been confirmed (Guizhou Bureau of Geology and Mineral Resources, 1990; Yunnan Bureau of Geology and Mineral Resources, 1990), and could have induced this second stage native copper mineralization (Fig. 8). Epithermal gold mineralization with an age range of 133 to 80 Ma has also been widely found in western Guizhou (Hu et al., 2003).

5. Conclusions

Evidence from mineral assemblages and geochemistry indicates that native copper mineralization in northeastern Yunnan was mainly related to moderate-temperature (200 to 350 °C) reducing fluids. Laumontites associated with native copper yield consistent ^{40}Ar/^{39}Ar plateau and isochron ages (226 to 228 Ma), in agreement with that of the Zn–Pb–Ag–Ge ores in this area, the major metallogenic event related with the Emeishan CFB. Heulandite yields a stable ^{40}Ar/^{39}Ar

plateau age of 134.0 ± 1.7 Ma, in agreement with the isochron ages of the U–Th–Pb isotopic system. This represents a second stage of hydrothermal activity that led to native copper mineralization over a temperature range of 100 to 200 °C.

References

Aja, S.U., Wood, S.A., Williams-Jones, A.E., 1995. The aqueous geochemistry of Zr and the solubility of some Zr-bearing minerals. Applied Geochemistry 10, 603–620.

Allen, D.E., Seyfried Jr., W.E., 2005. REE controls in ultramafic hosted MOR hydrothermal systems: an experimental study at elevated temperature and pressure. Geochimica et Cosmochimica Acta 69, 675–683.

Barker, C.E., Pawlewicz, M.J., 1986. The correlation of vitrinite reflectance with maximum temperature in humic organic matter. In: Buntebarth, G., Stegena, L. (Eds.), Paleogeothermics. Springer-Verlag, New York, pp. 79–93.

Bornhorst, T.J., Paces, J.B., Grant, N.K., Obradovich, J.D., Huber, N.K., 1988. Age of native copper mineralization, Keweenaw Peninsula, Michigan. Economic Geology 83, 619–625.

Boven, A., Pasteels, P., Punzalan, L.E., Liu, J., Luo, X., Zhang, W., Guo, Z., Hertogen, J., 2002. ^{40}Ar/^{39}Ar geochronological constraints on the age and evolution of the Permo-Triassic Emeishan Volcanic Province, Southwest China. Journal of Asian Earth Sciences 20, 157–175.

Carlos, J., Bradley, R.H., 1997. Experimental investigation of laumontite-wairakite-H2O: a model diagenetic reaction. American Mineralogist 82, 781–789.

Cannon, W.F., Nicholson, S.W., McRae, M.E., 1999. Geology and mineral deposits of the Keweenaw Peninsula, Michigan. United States Geological Survey Open File Report 99-149, 47 pp.

Carr, P.F., Pemberton, J.W., Nunan, E., 1999. Low-grade metamorphism of mafic lavas, upper Permian Brroughton Formation, Sydney Basin. Australian Journal of Earth Science 46, 839–849.

Davis, D.W., Paces, J.B., 1990. Time resolution of geologic events on the Keweenaw Peninsula and implications for development of the Midcontinent Rift System. Earth and Planetary Science Letters 97, 54–64.

Guizhou Bureau of Geology and Mineral Resources, 1990. Regional Geology of Guizhou Province. Geological Publishing House, Beijing. 698 pp. (in Chinese).

Haas, J.R., Shock, E.L., Sassani, D.C., 1995. Rare earth elements in hydrothermal systems: estimates of standard partial molal thermodynamic properties of aqueous complexes of the rare earth elements at high pressures and temperatures. Geochimica et Cosmochimica Acta 59, 4329–4350.

Hamilton, S.K., 1967. Copper mineralization in the upper part of the Copper Harbor conglomerate at White Pine, Michigan. Economic Geology 62, 885–904.

Ho, E.S., Mauk, J.L., 1996. Relationship between organic matter and copper mineralization in the Proterozoic Nonesuch Formation, northern Michigan. Ore Geology Reviews 11, 71–87.

Ho, E.S, Meyers, P.A., Mauk, J.L., 1990. Organic geochemical study of mineralization in the Keweenaw Nonesuch Formation at White Pine, Michigan. Organic Geochemistry 16, 229–234.

Hole, M.J., Trewin, N.H., Still, J., 1992. Mobility of the high field strength, rare earth elements and yttrium during late diagenesis. Journal of the Geological Society 149, 689–692.

Hu, R.Z., Wang, G.Z., Su, W.C., Peng, J.T., Bi, X.W., 2003. Discussion on genesis of a large domain of epithermal mineralization and related giant deposits in Southwest China. In: Zhao, Z.H., Tu, G.Z. (Eds.), Giant Deposits in China. Science Press, Beijing, pp. 267–300 (in Chinese).

Huang, Z.L., Chen, J., Han, R.S., Li, W.B., Liu, C.Q., Zhang, Z.L., Ma, D.Y., Gao, D.R., Yang, H.L., 2005. Geochemistry and Ore-formation of the Huize Giant Lead–Zinc Deposit, Yunnan Province, China: Discussion on the Relationship between Emeishan Flood Basalts and Lead–Zinc Mineralization. Geological Publishing House, Beijing. 187 pp. (in Chinese with English Abstract).

Jacob, H., 1989. Classification, structure, genesis and practical importance of natural solid oil bitumen ("migrabitumen"). International Coal Geology 11, 65–79.

Jenkins, D.M., Bozhilov, K.N., 2003. Stability and thermodynamic properties of ferro-actinolite: a re-investigation. American Journal of Science 303, 723–752.

Jiang, S.Y., 2000. Controls on the mobility of high field strength elements (HFSE), U, and Th in an ancient submarine hydrothermal system of the Proterozoic Sullivan Pb–Zn–Ag deposit, British Columbia, Canada. Geochemical Journal 34, 341–348.

Jiang, N., Sun, S.H., Chu, X.L., Mizuta, T., Ishiyama, D., 2003. Mobilization and enrichment of high-field strength elements during late- and post-magmatic processes in Shuiquangou syenitic complex, Northern China. Chemical Geology 200, 117–128.

Kamer, B.S., Collerson, K.D., 2000. Zr/Nb systematics of ocean island basalts reassessed—the case for binary mixing. Journal of Petrology 41, 1007–1021.

Lefebure, D.V., Church, B.N., 1996. Volcanic redbed Cu. In: Lefebure, D.V. (Ed.), Selected British Columbia Mineral Deposit Profiles, Volume 1, Metallic Deposits. Geological Survey of British Columbia Open File Report, vol. 13, pp. 5–7.

Li, H.M., Mao, J.W., Zhang, C.Q., Xu, H., Chen, Y.C., Wang, D.H., 2004. Isotopic geochemistry of Emeishan copper deposits in northeastern Yunnan and western Guizhou. Mineral Deposits 23, 232–240.

Lo, C.H., Chung, S.L., Lee, T.Y., Wu, G., 2002. Age of the Emeishan flood magmatism and relations to Permian–Triassic boundary events. Earth and Planetary Science Letters 198, 449–458.

McDougall, I., Harrison, M.T., 1988. Geochronology and Thermochronology by the ^{40}Ar/^{39}Ar Method. Clarendon Press, New York. 270 pp.

Smith, M.P., Henderson, P., Campbell, L.S., 2000. Fractionation of the REE during hydrothermal processes: constraints from the Bayan Obo Fe-REE-Nb deposit, Inner Mongolia, China. Geochimica et Cosmochimica Acta 64, 3141–3160.

Steiger, R.H., Jager, E., 1977. Subcommission on geochronology: convention on the use of decay constants in geo- and cosmochronology. Earth and Planetary Science Letters 36, 359–362.

Sueno, S., Cameron, M., Papike, J.J., Prewitt, C.T., 1973. The high temperature crystal chemistry of tremolite $T=400\,°C$. American Mineralogist 58, 649–664.

Todt, W., Cliff, R.A., Hanser, A., Hofmann, A.W., 1993. Re-calibration of NBS lead standards using a $^{202}Pb+^{205}Pb$ double spike. Terra Nova, Abstract Supplement 5, 396.

Wang, S.S., 1983. Age determinations of $^{40}Ar–^{40}K$, $^{40}Ar–^{39}Ar$ and radiogenic Ar released characteristics on geostandards of China. Chinese Journal of Geology 3, 315–323.

Whitney, P.R., Olmsted, J.F., 1998. Rare earth element metasomatism in hydrothermal system: the Willsboro-Lewis wollastonite ores, New York, USA. Geochimica et Cosmochimica Acta 62, 2965–2977.

Yunnan Bureau of Geology and Mineral Resources, 1990. Regional Geology of Yunnan. Geological Publishing House, Beijing. 728 pp.

Zheng, Y.F., 1993. Calculation of oxygen isotope fractionation in hydroxyl-bearing silicates. Earth and Planetary Science Letters 120, 247–263.

Zhou, M.F., Malpasa, J., Song, X.Y., Robinson, P.T., Sun, M., Kennedy, A.K., Lesher, C.M., Keays, R.R., 2002. A temporal link between the Emeishan large igneous province (SW China) and the end—Guadalupian mass extinction. Earth and Planetary Science Letters 196, 113–122.

Zhu, B.Q., Hu, Y.G., Zhang, Z.W., Chang, X.Y., 2003. Discovery of the copper deposits with features of the Keweenawan type in the border area of Yunnan–Guizhou Provinces. Science in China (ser. D) 46, 60–72 (suppl.).

Zhu, B.Q., Hu, Y.G., Chang, X.Y., Xie, J., Zhang, Z.W., 2005a. The Emeishan large igneous province originated from magmatism of a primitive mantle plus subducted slab. Russian Geology and Geophysics 46, 904–921.

Zhu, B.Q., Zhang, Z.W., Hu, Y.G., 2005b. Controls of magmatism and hydrothermal activities on mineralization in the Emeishan flood basalt province. In: Mao, J., Bierlein, F.P. (Eds.), Mineral Deposit Research: Meeting the Global Challenge. Springer-Verlag, Berlin-Heidelberg, pp. 77–80.